ACS Medicinal Chemistry Letters

pubs.acs.org/acsmedchemlett
Letter

A Hybrid Energy-Based and AI-Based Screening Approach for the Discovery of Novel Inhibitors of AXL

Xinting Lv, Youkun Kang, Xinglong Chi, Jingyi Zhao, Zhichao Pan, Xiaojun Ying, Long Li, Youlu Pan, Wenhai Huang,* and Linjun Wang*

Cite This: ACS Med. Chem. Lett. 2025, 16, 410−419
Read Online
ACCESS | Metrics & More | Article Recommendations | Supporting Information

ABSTRACT: AXL, part of the TAM receptor tyrosine kinase family, plays a significant role in the growth and survival of various tissues and tumors, making it a critical target for cancer therapy. This study introduces a novel high-throughput virtual screening (HTVS) methodology that merges an AI-enhanced graph neural network, PLANET, with a geometric deep learning algorithm, DeepDock. Using this approach, we identified potent AXL inhibitors from our database. Notably, compound **9**, with an IC_{50} of 9.378 nM, showed excellent inhibitory activity, suggesting its potential as a candidate for further research. We also performed molecular dynamics simulations to explore the interactions between compound **9** and AXL, providing insights for future enhancements. This hybrid screening method proves effective in finding promising AXL inhibitors, and advancing the development of new cancer therapies.

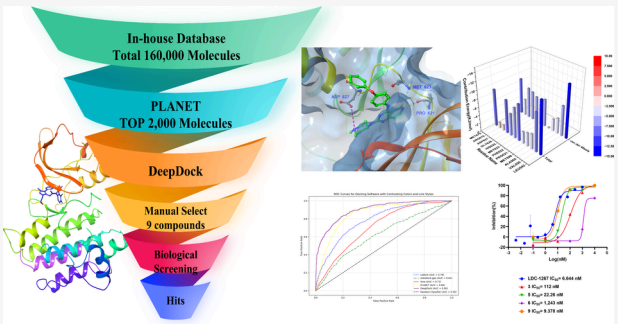

KEYWORDS: *AXL, Virtual screening, Bioactivity evaluation, Molecular dynamics, Geometric deep learning*

AXL (also known as Ark, Ufo, and Tyro-7) is a member of the TAM receptor tyrosine kinase family, which also includes Mer and Tyro-3.[1] Upon binding with the growth arrest-specific protein 6 (Gas6), AXL dimerizes and autophosphorylates, leading to the activation of downstream mitogen-activated protein kinase (MAPK) and phosphoinositide 3-kinase/protein kinase B (PI3K/AKT) pathways.[2] The cell outer membrane region of AXL contains two immunoglobulin repeat sequences (immunoglobulin and Ig) and two fibronectin type III domains (FNIII), which are the binding sites for endogenous ligands.[3]

It has been confirmed that the AXL is a key regulator of cell function which is associated with the growth of various tissues as well as the survival, proliferation and invasion of tumor cells. The prominent role of AXL in the development of various cancers has made it a drugable target for the treatment of cancers like glioblastoma multiforme[4] and acute myeloid leukemia.[5,6] The abundance of experimental data demonstrated that the downregulation of AXL can inhibit the growth of malignant tumors such as mesothelioma[7] and colorectal adenocarcinoma.[8] Meanwhile, overexpression of AXL in breast and pancreatic cancer was also significantly associated with the increased incidence of metastasis.[9,10] Additionally, AXL activation is also closely correlated with the expression of phosphorylated-AKT and matrix metalloprotein-9 (MMP9), promoting cell migration and invasion.[6]

At present, some active compounds targeting AXL have been on the market or in clinical studies (Figure 1).[11] Significantly, the small molecule inhibitors of AXL could be divided into two types according to the different binding modes. At present, the reported type I inhibitors include Bemcentinib (BGB324), Amuvatinib (MP-470), Dubermatinib (TP-0903), etc. It is worth noting that Bemcentinib is a highly specific and selective AXL inhibitor that has been studied extensively in a variety of cancer models, including breast, prostate, lung, pancreatic and ovarian cancers.[12] Besides, Foretinib (GSK1363089)[13] and Sitravatinib (MGCD516) (Figure 1) as the specific type II AXL inhibitors are also in different research phases.

The integration of computer-aided drug design (CADD)[14,15] employing sophisticated computational modeling techniques has markedly expedited the drug discovery process. This approach, notably through in silico screening, has become a pivotal tool in enhancing the efficiency of drug discovery and development. The application of deep learning models, such as PLANET and DeepDock, in predicting molecular activity has demonstrated considerable promise. These models adeptly predict binding affinities and conformations of molecules by learning the intricate interactions

Received: October 23, 2024
Revised: January 7, 2025
Accepted: January 7, 2025
Published: February 10, 2025

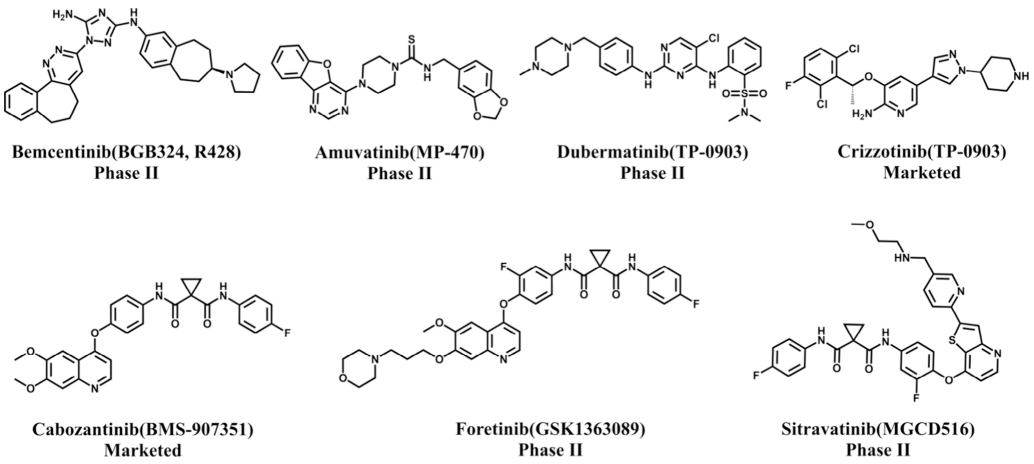

Figure 1. Structures of reported AXL inhibitors.

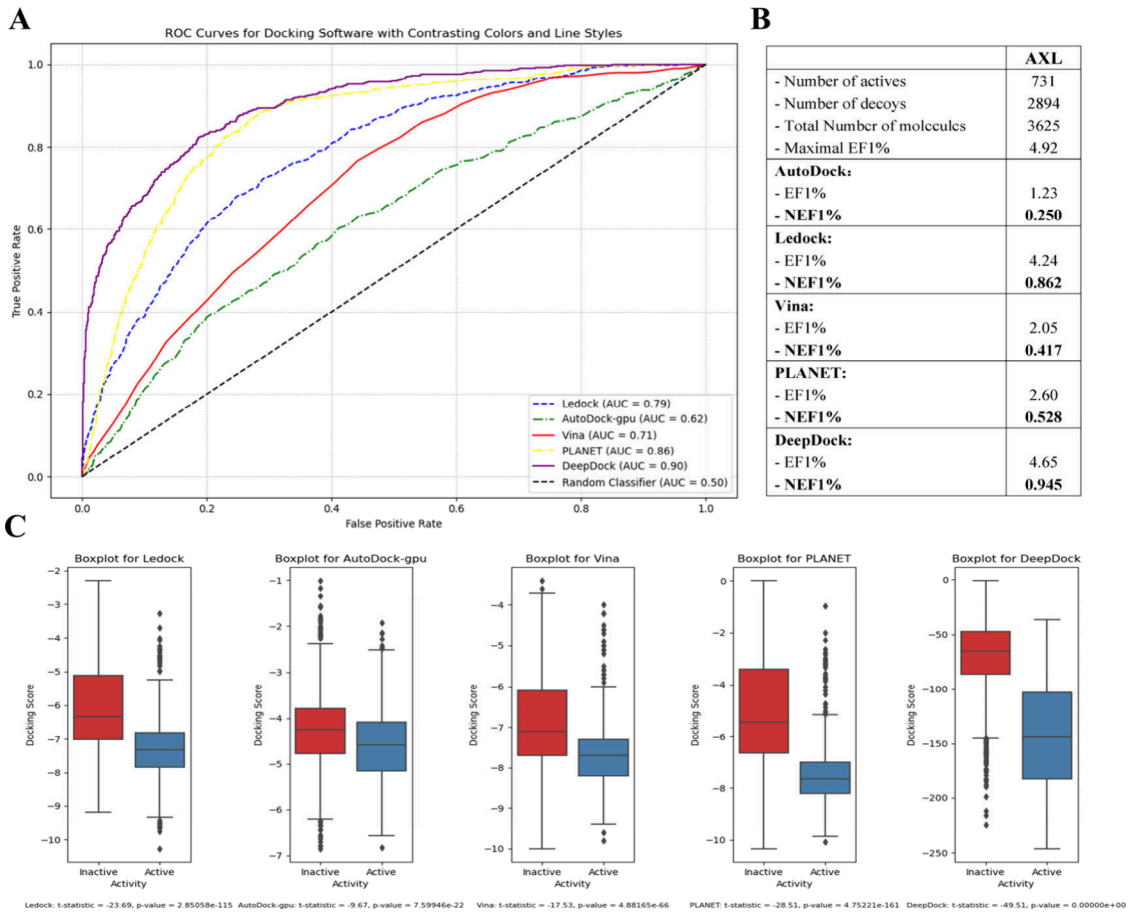

	AXL
- Number of actives	731
- Number of decoys	2894
- Total Number of molecules	3625
- Maximal EF1%	4.92
AutoDock:	
- EF1%	1.23
- NEF1%	**0.250**
Ledock:	
- EF1%	4.24
- NEF1%	**0.862**
Vina:	
- EF1%	2.05
- NEF1%	**0.417**
PLANET:	
- EF1%	2.60
- NEF1%	**0.528**
DeepDock:	
- EF1%	4.65
- NEF1%	**0.945**

Figure 2. Evaluation results of virtual screening software. (A) The ROC curve for the molecular docking of the DUD-E data set into the selected receptor conformations with the selected docking programs: (B) The EF1% and NEF1% assessment of the selected software on the data set; (C) the *t* test and boxplot of the validation for selected software.

between proteins and ligands, thus not only streamlining the drug candidate screening process but also bolstering the discovery of potential drugs with novel structures and significant inhibitory activity.

In our research, we crafted a virtual screening workflow tailored to discover novel compounds with the potential to inhibit AXL. Initially, we established an "in-house" database, incorporating a variety of compounds from both the Maybridge and MCE drug-like compound libraries. We employed PLANET, a sophisticated AI-powered graph neural network algorithm, as our primary tool for the initial screening phase. Following the screening, we carefully selected candidates based on the DeepDock, which led to the identification of nine compounds exhibiting inhibitory properties against AXL. Notably, compound **9** demonstrated considerable inhibitory activity, evidenced by an IC_{50} value of 9.378 nM. To further understand the dynamic interaction between compound **9** and AXL, we undertook molecular

https://doi.org/10.1021/acsmedchemlett.4c00511
ACS Med. Chem. Lett. 2025, 16, 410−419

dynamics simulations. The analysis of these simulations allowed us to examine the stability of the compound **9**−AXL complex, observe conformational changes over time, and identify critical interactions that influence the binding affinity. This comprehensive analysis not only highlights the distinct binding features of compound **9** to AXL but also offers essential insights for the ongoing development and enhancement of AXL inhibitors.

The X-ray structure of AXL (PDB 5U6B) was from RCSB Protein Data Bank (www.rcsb.org),[16] which was applied in further analysis via the Rosetta 3.13 suite.[17,18] All nonprotein at-oms were removed, and residue renumbering and format conversion were performed on the AXL protein following the default parameters without further modification. The protein structures were subsequently converted to PDBQT format using AutoDockTools (version 1.5.7)[19−21] and OpenBabel,[22] which involved assigning atomic partial charges and specific atom types. By applying these rigorous procedures, we ensured reliable and efficient use of the AXL protein structure for further analysis in this study.

Molecular diversity[23,24] is a crucial element in virtual screening, as it has been demonstrated to significantly contribute to achieving high hit rates. To augment the molecular diversity within our compound libraries, we combined the Maybridge Compound Library with MCE's drug-like molecule library to create an "in-house" database. For further refinement of this database, we employed AutoDock and Open Babel software. These tools were used to generate 3D structures of the library's compounds, verify their correct protonation states, and confirm their appropriate molecular formats. Such preparation of the "in-house" database was instrumental in enhancing its structural reliability and precision, thereby substantially improving the prospects of effective virtual screening outcomes.

Molecular docking is a fundamental technique in the field of modern structural drug design, widely employed for its computational efficiency and accuracy. Its principal function is to ascertain the most favorable conformation of a ligand within the active site of a target protein, as well as to estimate the strength of the interaction between the protein and the ligand. With the advent of artificial intelligence, AI-based prediction tools have become increasingly significant. These tools, adept at analyzing extensive data sets of molecular and protein interactions, are able to predict the binding modes and affinities of ligands to proteins with enhanced precision. In addition, Selecting the right molecular docking software is a critical factor in conducting effective virtual screening. We conducted a comprehensive evaluation of various software options for our specific research needs, including AutoDock-GPU,[21,25] AutoDock-Vina,[26,27] LeDock,[28] PLANET,[29] and DeepDock.[30] Then We obtained a high-quality data set of comet molecules with pIC_{50} values > = 6 from the ChEMBL database[31−33] and clustered them into 50 groups. A decoy data set was generated using DUD-E[34−36] to serve as an evaluation data set for docking software. The data sets were then converted into the required file formats using AutoDock Tools and Open Babel. The findings of this evaluation, which are comprehensively detailed in Figure 2, were focused on identifying software that guarantees the highest levels of accuracy and reliability in our virtual screening process. The area under the receiver operating characteristic (ROC) curve is a crucial metric in evaluating the discriminative power of a model, particularly in differentiating between active and inactive (or decoy) data. In Figure 2A, DeepDock and PLANET demonstrated superior performance, as indicated by their substantial areas under the ROC curve, with AUC values of 0.90 and 0.86, respectively. These results signify that DeepDock and PLANET possess the most effective discrimination capabilities when it comes to distinguishing between the active and decoy data sets specific to AXL (Figure 2A−C). Based on these findings, we decided to integrate DeepDock and PLANET into our virtual screening workflow.

Then the high-throughput virtual screening (HTVS) was employed to identify potential target molecules, utilizing our "in-house" compound database in conjunction with prepre-pared AXL protein structures. Our database comprises a total of 160 000 small molecules, providing an ample selection for our screening purposes. The virtual screening workflow is depicted in Figure 3. Initially, molecules from the internal

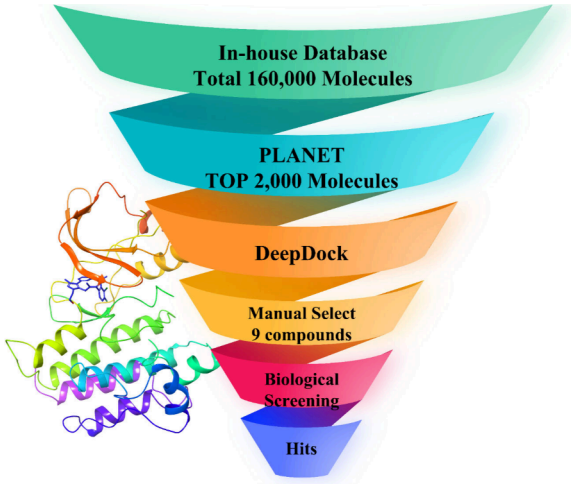

Figure 3. HTVS workflow for discovering AXL inhibitors.

database were filtered through the PLANET program, leading to the shortlisting of 2000 molecules with a PLANET affinity of 6.782 or higher. These molecules were then subjected to further screening using the DeepDock algorithm, which evaluated the influence of various atoms on target binding and facilitated the manual selection process. Subsequently, experienced medicinal chemists conducted an assessment of these molecules, focusing on high binding affinity and potential druggability, possibly leading to the exclusion of some molecules. The selection process culminated in the identification of nine compounds, as detailed in Figure 4 and Table 1.

Following the HTVS results, nine selected compounds (each at 25 μM concentration) were further assessed for their inhibition rates against AXL. As shown in Figure 5A, compounds **3**, **5**, **6**, and **9** exhibited higher inhibition rates compared to the rest. Consequently, the IC_{50} values of these four compounds on AXL were further determined. Remarkably, compound **9** exhibited superior inhibitory activity to AXL (IC_{50} = 9.38 nM). Additionally, compounds **3** (IC_{50} = 112.0 nM) and **5** (IC_{50} = 22.3 nM) also demonstrated commendable inhibitory activities (Figure 5B). This collective analysis not only validates the efficacy of our HTVS process but also lays a solid foundation for the advancement of innovative AXL inhibitors.

Building on the inhibitory activity assessments, the molecular dynamics (MD) simulation of compound **9** with

https://doi.org/10.1021/acsmedchemlett.4c00511
ACS Med. Chem. Lett. 2025, 16, 410−419

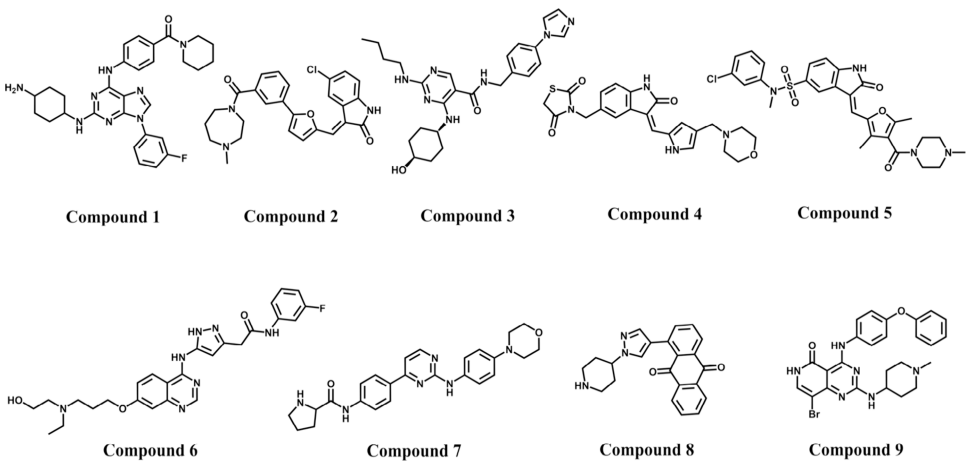

Figure 4. Nine screened compounds after HTVS.

Table 1. Docking Score of Nine Selected Compounds

compd	PLANET affinity	DeepDock score	similarity score	inhibition rate (%)
1	9.756	−150.448	0.386	96.77 ± 1.12
2	7.790	−180.102	0.312	61.69 ± 6.06
3	7.323	−83.749	1.000	103.69 ± 1.81
4	7.127	−114.445	1.000	94.14 ± 1.81
5	7.975	−223.708	0.382	99.65 ± 0.11
6	6.884	−94.664	0.305	94.58 ± 3.83
7	7.439	−184.552	0.415	64.50 ± 4.13
8	6.822	−73.242	0.304	66.97 ± 1.76
9	7.591	−211.992	0.377	94.27 ± 1.82

AXL was carried out to interpret the interaction, which would inform further structural optimization efforts using Gromacs 2021.06.[37,38] The simulation, as depicted in Figure 7A, showed that after 500 ns, the binding of the protein and compound **9** stabilized, indicating a reliable complex for in-depth rational analysis. The last conformation was extracted for detailed examination.

As illustrated in Figure 6A,B, compound **9** aligns well within the binding pocket of the AXL protein, forming hydrogen bonds with critical residues PRO621, MET623, and ASP627. Further analysis using the free energy surface (FES) validated the stability of these binding interactions (Figure 6D). The FES plot depicts the relationship between the root-mean-square deviation (RMSD), radius of gyration (Rg), and free energy. Results indicate that upon binding to AXL, the system stabilizes in a low-free-energy region (shown in deep blue), signifying the strong binding affinity of this conformation (RMSD of 0.25 A, Rg of 1.92 nm).). The free energy minimum highlights the robust and stable interaction between compound **9** and AXL. This observation is further corroborated by the binding free energy calculated using the MM/PBSA method,[39−41] which yielded a value of −203.719 kJ/mol (Figure 6C), confirming the strength of the interaction. Figure 7B provides a detailed breakdown of the binding free energy contributions of individual residues involved in the interaction between compound **9** and AXL. Notably, residues MET623 and ASP627 were identified as significant contributors to the binding affinity. Moreover, parts C and D of Figure 7 analyze fluctuations in the distances between compound **9** and residues PRO621, MET623, and ASP627 throughout the simulation. These results demonstrate that these distances remain relatively stable during the simulation, further reinforcing the strong binding affinity between compound **9** and AXL. This stability aligns with the earlier hydrogen bond analysis, affirming the robustness of the binding mode.

By integrating free energy surface analysis, residue interaction data, and binding free energy calculations, we gained a comprehensive understanding of the dynamic behavior and interaction mechanism between compound **9** and AXL. These findings not only validate the reliability of the simulation results but also provide valuable insights for the rational optimization of compound **9**. Specifically, understanding the key residue contributions and stability of binding interactions will guide the design of derivatives with enhanced binding affinity and improved drug-like properties.

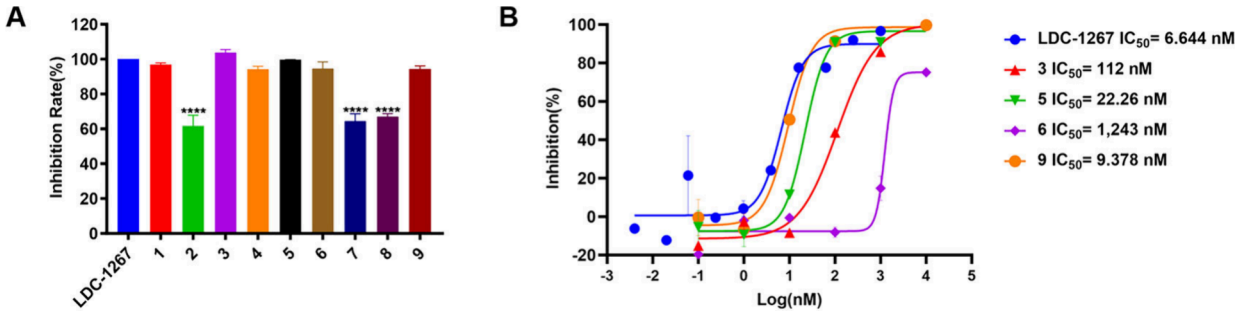

Figure 5. Biological evaluation results of screened compounds. (A) The inhibition rate (%) assay of nine selected compounds against AXL (LDC-1267 was the positive control). (B) The IC_{50} assessment of selected compounds (**3**, **5**, **6**, and **9**).

https://doi.org/10.1021/acsmedchemlett.4c00511
ACS Med. Chem. Lett. 2025, 16, 410−419

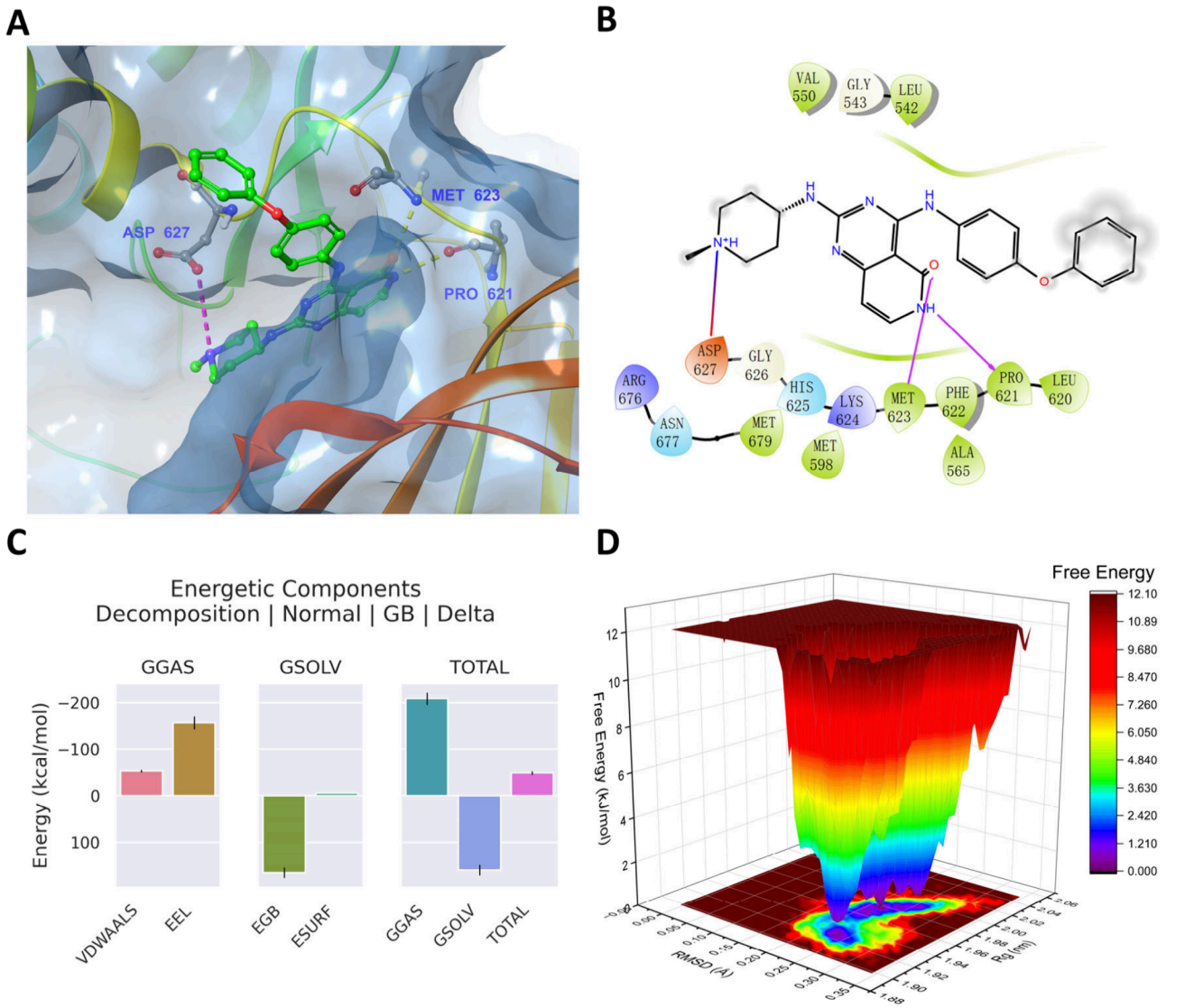

Figure 6. Binding detail analysis of AXL−compound **9** complex after MD. (A) The 3D binding mode of compound **9** and AXL protein. (B) The 2D diagram of interaction of compound **9** with AXL (purple: hydrogen bond; gradient from red to blue: salt bridge). (C) The energy analysis of compound **9** with AXL after 500 ns MD simulation. (D) The Gibbs freedom energy landscape of complex of compound **9** and AXL protein.

Subsequently, we conducted similarity search scoring and absorption, distribution, metabolism, and excretion and toxicity (ADMET) property predictions for the nine screened molecules (Table 1, Table 2, and Figure 8). As shown in Table 1, two of the screened molecules were identified as known AXL inhibitors, while the remaining candidate compounds displayed low structural similarity to previously known inhibitors. This outcome underscores the effectiveness and accuracy of our screening protocol, which successfully recognized established AXL inhibitors and, at the same time, identified novel candidates with AXL-inhibitory potential. By selecting both known inhibitors and structurally diverse new candidates, the protocol demonstrates its capability not only to confirm known inhibitor activity but also to expand the scope for discovering structurally novel compounds with AXL-targeting potential. The protocol's ability to detect known AXL inhibitors provides validation for its reliability and accuracy. That the screening process successfully identified molecules already recognized for their AXL-inhibitory activity suggests that it is sensitive to the key structural and functional characteristics of effective AXL inhibitors. This reliability is essential, as it assures that the protocol can be trusted to identify compounds with genuine therapeutic relevance. Furthermore, the discovery of structurally novel compounds with potential AXL-inhibitory properties indicates that the protocol is not solely dependent on structural similarity.

While we conducted ADMET property predictions for the nine screened molecules using admerSAR 3.0.[42] As described in Table 2 and Figure 7, compounds **1**−**9** exhibit relatively high SlogP values, indicating potentially excessive hydrophobicity, which may hinder their distribution and metabolism in vivo. Additionally, their quantitative estimate of drug-likeness (QED), a comprehensive metric ranging from 0 to 1 that assesses a molecule's "drug-likeness", is generally low. This suggests suboptimal drug-like properties, possibly due to predicted high-risk profiles for drug-induced liver injury (DILI) in some compounds. Specifically, compound **9**, identified as the most promising potential AXL inhibitor among the screened compounds, would benefit from structural modifications aimed at enhancing its water solubility, reducing

https://doi.org/10.1021/acsmedchemlett.4c00511
ACS Med. Chem. Lett. 2025, 16, 410−419

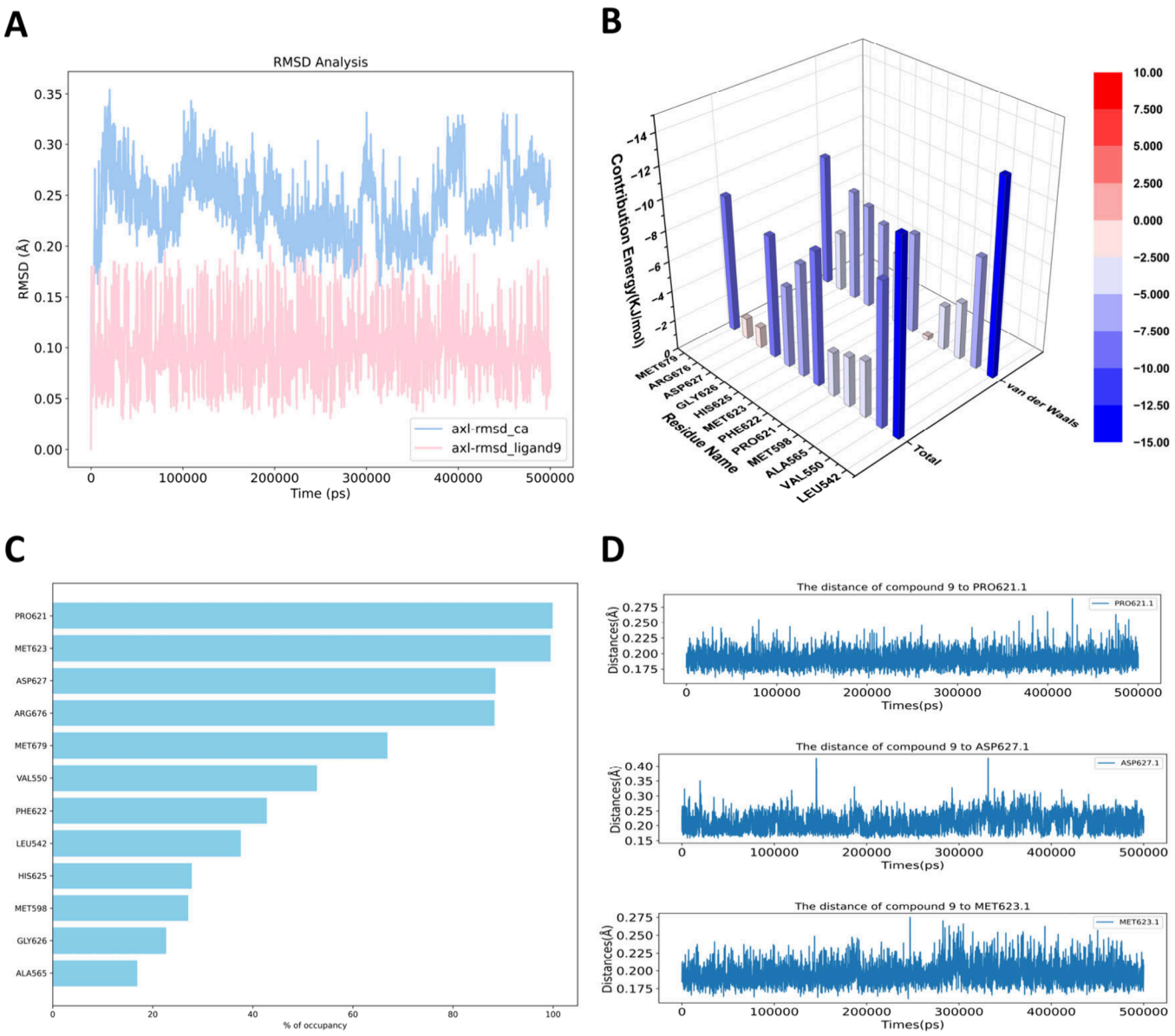

Figure 7. MD trajectory detail analysis of AXL−compound **9** complex. (A) RMSD values trajectory of compound **9** and AXL protein for 500 ns. (B) The residue energy contribution of compound **9**−AXL complex. (C) The occupancy percentage and (D) binding distances between compound **9** and different AXL residues.

Table 2. ADMET Prediction Results of Nine Screened Compounds

compd	SlogP	QED	pK_a	BBB	T50	DILI
1	5.006	0.322	accept	0.889	0.578	−1.869
2	4.870	0.565	accept	0.874	0.604	−1.317
3	3.520	0.340	3.272	0.938	0.412	−2.571
4	2.535	0.697	1.268	0.696	0.557	−2.307
5	3.990	0.454	3.194	0.500	0.738	−2.718
6	3.500	0.203	3.577	0.815	0.519	−2.749
7	3.414	0.537	3.010	0.971	0.124	−2.745
8	3.250	0.598	2.740	0.779	0.567	−2.195
9	5.123	0.324	accept	0.727	0.738	−1.624

hepatic and renal toxicity, and extending its half-life to improve its overall drug-like profile.

For compound **9**, the relatively high SlogP value may contribute to poor water solubility, which could limit its bioavailability and make it challenging to achieve effective plasma concentrations. Excessive hydrophobicity is also associated with a higher risk of accumulating in lipid-rich tissues, potentially leading to toxicity or undesirable side effects. Adjusting functional groups to increase polarity could help mitigate these issues, thus improving solubility and tissue distribution. Furthermore, the low QED score suggests that compound **9**'s molecular structure may lack certain features typical of drug-like molecules, such as balanced lipophilicity and lower predicted toxicity.

Predictions of high DILI risk highlight the importance of minimizing hepatic toxicity during optimization. Reducing specific structural motifs that may trigger liver injury or employing bioisosteric replacements to decrease metabolic reactivity could enhance compound **9**'s safety profile. Similarly, renal toxicity risk should be considered, as accumulation in the kidneys can lead to adverse renal effects, compromising the compound's therapeutic potential.

https://doi.org/10.1021/acsmedchemlett.4c00511
ACS Med. Chem. Lett. 2025, 16, 410−419

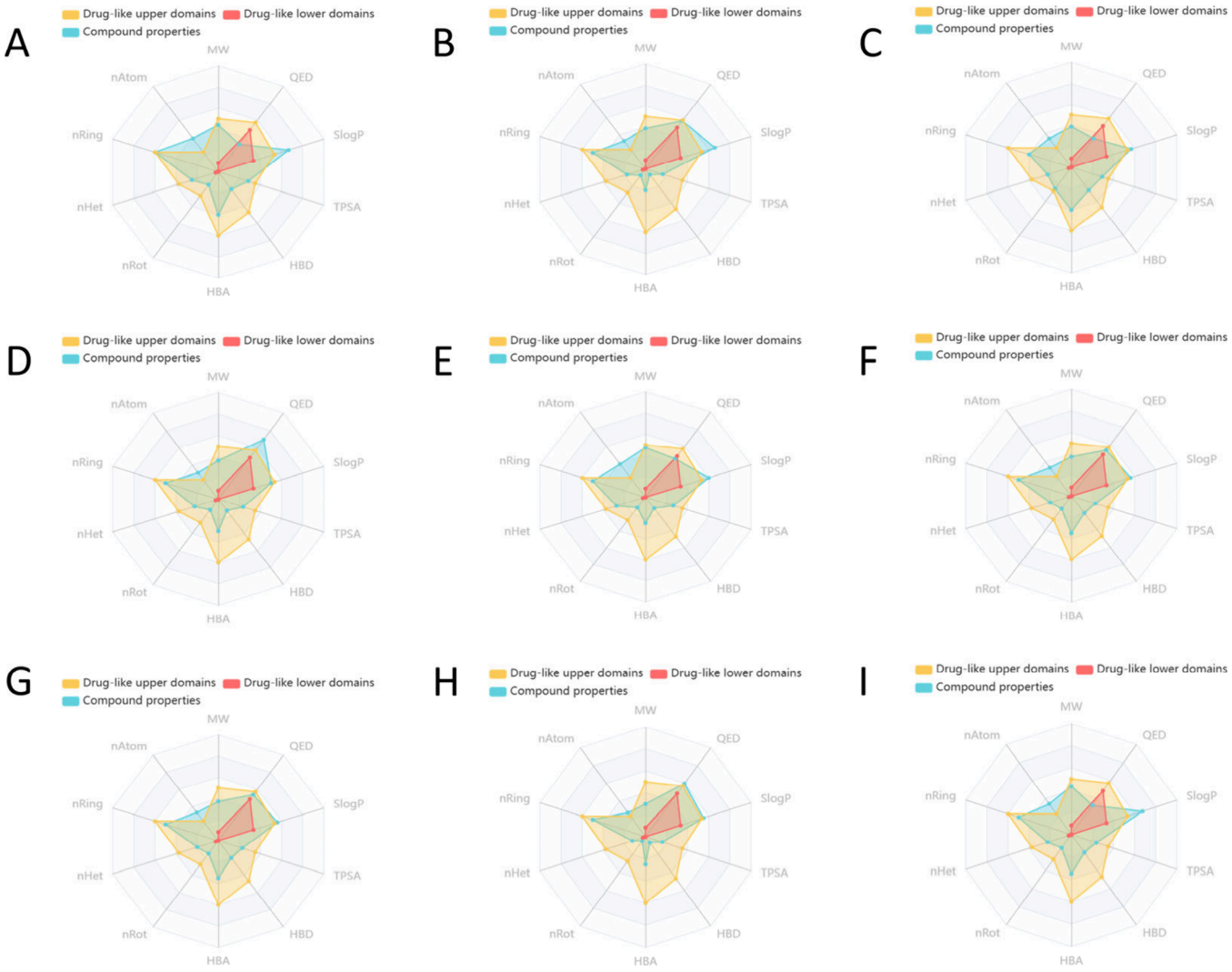

Figure 8. ADMET prediction results of nine screened molecules. (A) The radar chart of compound **1**. (B) The radar chart of compound **2**. (C) The radar chart of compound **3**. (D) The radar chart of compound **4**. (E) The radar chart of compound **5**. (F) The radar chart of compound **6**. (G) The radar chart of compound **7**. (H) The radar chart of compound **8**. (I) The radar chart of compound **9**.

Lastly, an extended half-life could enhance compound **9**'s pharmacokinetic profile, reducing the need for frequent dosing and improving patient compliance. Strategies to achieve this may include increasing metabolic stability through structural adjustments, which can lower clearance rates and prolong systemic circulation. In summary, optimizing compound **9** by addressing hydrophobicity, DILI risk, renal toxicity, and half-life could substantially improve its drug-likeness and therapeutic viability as a candidate AXL inhibitor.

Given the critical role of AXL overexpression in various cancers, the search for effective compounds targeting AXL has become increasingly significant in related disease research. The integration of virtual screening with artificial intelligence has risen to prominence in drug discovery, offering a cost-effective and efficient approach.

In our investigation, we designed a virtual screening workflow to identify potent, novel inhibitors of AXL. By employing advanced algorithms such as PLANET and DeepDock, we identified compound **9** as a highly effective AXL inhibitor, exhibiting significant inhibitory bioactivity (IC_{50} = 9.378 nM). Further exploration through molecular dynamics (MD) simulation revealed compound **9**'s specific binding mode to AXL. Notably, compound **9** forms stable hydrogen bond interactions with PRO621, MET623, and ASP627 within AXL, contributing to its high inhibitory potency. Additionally, compound **9** establishes robust hydrophobic interactions with VAL550, PHE622, GLY626, and MET679. These critical interactions between compound **9** and AXL offer insightful implications for the discovery and advancement of highly active AXL inhibitors, providing a foundation for future efforts in structural optimization and drug development.

Safety statement: All experiments involving hazardous materials were conducted following institutional and governmental safety guidelines. Proper personal protective equipment (PPE) was used throughout the study, and all waste was disposed of in compliance with environmental regulations.

■ ASSOCIATED CONTENT

Supporting Information

The Supporting Information is available free of charge at https://pubs.acs.org/doi/10.1021/acsmedchemlett.4c00511.

https://doi.org/10.1021/acsmedchemlett.4c00511
ACS Med. Chem. Lett. 2025, 16, 410−419

Experimental procedures; docking score of whole virtual screening; purity data of screened compounds; spectrum of screened compounds (PDF)

AUTHOR INFORMATION

Corresponding Authors

Linjun Wang − *Affiliated Yongkang First People's Hospital and School of Pharmaceutical Sciences, Hangzhou Medical College, Hangzhou 310053, P.R. China*; Email: 352671125@163.com

Wenhai Huang − *Affiliated Yongkang First People's Hospital and School of Pharmaceutical Sciences, Hangzhou Medical College, Hangzhou 310053, P.R. China; Key Laboratory of Neuropsychiatric Drug Research of Zhejiang Province, School of Pharmacy, Hangzhou Medical College, Hangzhou, Zhejiang 310000, P.R. China*; orcid.org/0000-0003-1457-7380; Email: hwh@hmc.edu.cn

Authors

Xinting Lv − *Affiliated Yongkang First People's Hospital and School of Pharmaceutical Sciences, Hangzhou Medical College, Hangzhou 310053, P.R. China; Key Laboratory of Neuropsychiatric Drug Research of Zhejiang Province, School of Pharmacy, Hangzhou Medical College, Hangzhou, Zhejiang 310000, P.R. China*

Youkun Kang − *Affiliated Yongkang First People's Hospital and School of Pharmaceutical Sciences, Hangzhou Medical College, Hangzhou 310053, P.R. China; Key Laboratory of Neuropsychiatric Drug Research of Zhejiang Province, School of Pharmacy, Hangzhou Medical College, Hangzhou, Zhejiang 310000, P.R. China*

Xinglong Chi − *Affiliated Yongkang First People's Hospital and School of Pharmaceutical Sciences, Hangzhou Medical College, Hangzhou 310053, P.R. China; Key Laboratory of Neuropsychiatric Drug Research of Zhejiang Province, School of Pharmacy, Hangzhou Medical College, Hangzhou, Zhejiang 310000, P.R. China*

Jingyi Zhao − *College of Pharmaceutical Sciences, Zhejiang University, Hangzhou 310058, China*

Zhichao Pan − *College of Pharmaceutical Sciences, Zhejiang University, Hangzhou 310058, China*

Xiaojun Ying − *Affiliated Yongkang First People's Hospital and School of Pharmaceutical Sciences, Hangzhou Medical College, Hangzhou 310053, P.R. China*

Long Li − *Affiliated Yongkang First People's Hospital and School of Pharmaceutical Sciences, Hangzhou Medical College, Hangzhou 310053, P.R. China*

Youlu Pan − *Affiliated Yongkang First People's Hospital and School of Pharmaceutical Sciences, Hangzhou Medical College, Hangzhou 310053, P.R. China; Key Laboratory of Neuropsychiatric Drug Research of Zhejiang Province, School of Pharmacy, Hangzhou Medical College, Hangzhou, Zhejiang 310000, P.R. China*

Complete contact information is available at: https://pubs.acs.org/10.1021/acsmedchemlett.4c00511

Author Contributions

Xinting Lv, Youkun Kang, and Xinglong Chi contributed equally to this work. The manuscript was written through contributions of all authors. Xinting Lv: Writing—review and editing. Youkun Kang: Writing—original draft preparation. Xinglong Chi: Writing—original draft preparation. Jingyi Zhao: Writing—review and editing, Methodology. Zhichao Pan: Software and data analysis. Xiaojun Ying: Validation and formal analysis. Long Li: Resources. Youlu Pan: Project administration. Wenhai Huang: Visualization and software. Linjun Wang: Conceptualization and methodology. All authors have read and agreed to the published version of the manuscript. All authors have given approval to the final version of the manuscript.

Notes

The authors declare no competing financial interest.

ACKNOWLEDGMENTS

This study was funded by the Zhejiang Provincial Medical and Health Science and Technology Program (2022RC289). We express our sincere appreciation for the support and services rendered by lCE Bioscience Inc. The biological activity testing conducted by their team played a crucial role in the research detailed in this publication. We sincerely thank Jianwei Pan for his valuable contributions during the revision process of this manuscript.

ABBREVIATIONS

AXL, Anexelekto; AUC, area under the curve; GAFF, generalized AMBER force field; MD, molecular dynamics; RMSD, root-mean square deviation; Rg, radius of gyration; MM/PBSA, molecular mechanics/Poisson−Boltzmann surface area; CCK-8, Cell counting kit-8; OD, optical density

REFERENCES

(1) Hafizi, S.; Dahlback, B. Signalling and functional diversity within the Axl subfamily of receptor tyrosine kinases. *Cytokine Growth Factor Rev.* **2006**, *17* (4), 295−304.

(2) Sen, T.; Tong, P.; Diao, L.; Li, L.; Fan, Y.; Hoff, J.; Heymach, J. V.; Wang, J.; Byers, L. A. Targeting AXL and mTOR Pathway Overcomes Primary and Acquired Resistance to WEE1 Inhibition in Small-Cell Lung Cancer. *Clin. Cancer Res.* **2017**, *23* (20), 6239−6253.

(3) Zhu, C.; Wei, Y.; Wei, X. AXL receptor tyrosine kinase as a promising anti-cancer approach: functions, molecular mechanisms and clinical applications. *Mol. Cancer* **2019**, *18* (1), 153.

(4) Hutterer, M.; Knyazev, P.; Abate, A.; Reschke, M.; Maier, H.; Stefanova, N.; Knyazeva, T.; Barbieri, V.; Reindl, M.; Muigg, A.; Kostron, H.; Stockhammer, G.; Ullrich, A. Axl and growth arrest-specific gene 6 are frequently overexpressed in human gliomas and predict poor prognosis in patients with glioblastoma multiforme. *Clin. Cancer Res.* **2008**, *14* (1), 130−8.

(5) Ben-Batalla, I.; Schultze, A.; Wroblewski, M.; Erdmann, R.; Heuser, M.; Waizenegger, J. S.; Riecken, K.; Binder, M.; Schewe, D.; Sawall, S.; Witzke, V.; Cubas-Cordova, M.; Janning, M.; Wellbrock, J.; Fehse, B.; Hagel, C.; Krauter, J.; Ganser, A.; Lorens, J. B.; Fiedler, W.; Carmeliet, P.; Pantel, K.; Bokemeyer, C.; Loges, S. Axl, a prognostic and therapeutic target in acute myeloid leukemia mediates paracrine crosstalk of leukemia cells with bone marrow stroma. *Blood* **2013**, *122* (14), 2443−52.

(6) Han, J.; Tian, R.; Yong, B.; Luo, C.; Tan, P.; Shen, J.; Peng, T. Gas6/Axl mediates tumor cell apoptosis, migration and invasion and predicts the clinical outcome of osteosarcoma patients. *Biochem. Biophys. Res. Commun.* **2013**, *435* (3), 493−500.

(7) Ou, W. B.; Corson, J. M.; Flynn, D. L.; Lu, W. P.; Wise, S. C.; Bueno, R.; Sugarbaker, D. J.; Fletcher, J. A. AXL regulates mesothelioma proliferation and invasiveness. *Oncogene* **2011**, *30* (14), 1643−52.

(8) Yuen, H. F.; McCrudden, C. M.; Huang, Y. H.; Tham, J. M.; Zhang, X.; Zeng, Q.; Zhang, S. D.; Hong, W. TAZ expression as a prognostic indicator in colorectal cancer. *PLoS One* **2013**, *8* (1), No. e54211.

(9) Gjerdrum, C.; Tiron, C.; Hoiby, T.; Stefansson, I.; Haugen, H.; Sandal, T.; Collett, K.; Li, S.; McCormack, E.; Gjertsen, B. T.; Micklem, D. R.; Akslen, L. A.; Glackin, C.; Lorens, J. B. Axl is an essential epithelial-to-mesenchymal transition-induced regulator of breast cancer metastasis and patient survival. *Proc. Natl. Acad. Sci. U. S. A.* **2010**, *107* (3), 1124−9.
(10) Koorstra, J.-B. M.; Karikari, C.; Feldmann, G.; Bisht, S.; Leal-Rojas, P.; Offerhaus, G. J. A.; Alvarez, H.; Maitra, A. The Axl receptor tyrosine kinase confers an adverse prognostic influence in pancreatic cancer and represents a new therapeutic target. *Cancer Biol. Ther* **2009**, *8* (7), 618.
(11) Zhang, Z.; Lee, J. C.; Lin, L.; Olivas, V.; Au, V.; LaFramboise, T.; Abdel-Rahman, M.; Wang, X.; Levine, A. D.; Rho, J. K.; Choi, Y. J.; Choi, C. M.; Kim, S. W.; Jang, S. J.; Park, Y. S.; Kim, W. S.; Lee, D. H.; Lee, J. S.; Miller, V. A.; Arcila, M.; Ladanyi, M.; Moonsamy, P.; Sawyers, C.; Boggon, T. J.; Ma, P. C.; Costa, C.; Taron, M.; Rosell, R.; Halmos, B.; Bivona, T. G. Activation of the AXL kinase causes resistance to EGFR-targeted therapy in lung cancer. *Nat. Genet.* **2012**, *44* (8), 852−60.
(12) Tanaka, M.; Siemann, D. W. Therapeutic Targeting of the Gas6/Axl Signaling Pathway in Cancer. *Int. J. Mol. Sci.* **2021**, *22* (18), 9953.
(13) Eder, J. P.; Shapiro, G. I.; Appleman, L. J.; Zhu, A. X.; Miles, D.; Keer, H.; Cancilla, B.; Chu, F.; Hitchcock-Bryan, S.; Sherman, L.; McCallum, S.; Heath, E. I.; Boerner, S. A.; LoRusso, P. M. A phase I study of foretinib, a multi-targeted inhibitor of c-Met and vascular endothelial growth factor receptor 2. *Clin. Cancer Res.* **2010**, *16* (13), 3507−16.
(14) Cui, W.; Aouidate, A.; Wang, S.; Yu, Q.; Li, Y.; Yuan, S. Discovering Anti-Cancer Drugs via Computational Methods. *Front Pharmacol* **2020**, *11*, 733.
(15) Lee, J. W.; Maria-Solano, M. A.; Vu, T. N. L.; Yoon, S.; Choi, S. Big data and artificial intelligence (AI) methodologies for computer-aided drug design (CADD). *Biochem. Soc. Trans.* **2022**, *50* (1), 241−252.
(16) Goodsell, D. S.; Zardecki, C.; Di Costanzo, L.; Duarte, J. M.; Hudson, B. P.; Persikova, I.; Segura, J.; Shao, C.; Voigt, M.; Westbrook, J. D.; Young, J. Y.; Burley, S. K. RCSB Protein Data Bank: Enabling biomedical research and drug discovery. *Protein Sci.* **2020**, *29* (1), 52−65.
(17) Leaver-Fay, A.; Tyka, M.; Lewis, S. M.; Lange, O. F.; Thompson, J.; Jacak, R.; Kaufman, K.; Renfrew, P. D.; Smith, C. A.; Sheffler, W.; Davis, I. W.; Cooper, S.; Treuille, A.; Mandell, D. J.; Richter, F.; Ban, Y. E.; Fleishman, S. J.; Corn, J. E.; Kim, D. E.; Lyskov, S.; Berrondo, M.; Mentzer, S.; Popovic, Z.; Havranek, J. J.; Karanicolas, J.; Das, R.; Meiler, J.; Kortemme, T.; Gray, J. J.; Kuhlman, B.; Baker, D.; Bradley, P. ROSETTA3: an object-oriented software suite for the simulation and design of macromolecules. *Methods Enzymol* **2011**, *487*, 545−74.
(18) Shorthouse, D.; Hall, M. W. J.; Hall, B. A. Computational Saturation Screen Reveals the Landscape of Mutations in Human Fumarate Hydratase. *J. Chem. Inf Model* **2021**, *61* (4), 1970−1980.
(19) El-Hachem, N.; Haibe-Kains, B.; Khalil, A.; Kobeissy, F. H.; Nemer, G. AutoDock and AutoDockTools for Protein-Ligand Docking: Beta-Site Amyloid Precursor Protein Cleaving Enzyme 1(BACE1) as a Case Study. *Methods Mol. Biol.* **2017**, *1598*, 391−403.
(20) Forli, S.; Huey, R.; Pique, M. E.; Sanner, M. F.; Goodsell, D. S.; Olson, A. J. Computational protein-ligand docking and virtual drug screening with the AutoDock suite. *Nat. Protoc* **2016**, *11* (5), 905−19.
(21) Santos-Martins, D.; Solis-Vasquez, L.; Tillack, A. F.; Sanner, M. F.; Koch, A.; Forli, S. Accelerating AutoDock4 with GPUs and Gradient-Based Local Search. *J. Chem. Theory Comput* **2021**, *17* (2), 1060−1073.
(22) O'Boyle, N. M.; Banck, M.; James, C. A.; Morley, C.; Vandermeersch, T.; Hutchison, G. R. Open Babel: An open chemical toolbox. *J. Cheminform* **2011**, *3*, 33.
(23) Ferreira, L. G.; Dos Santos, R. N.; Oliva, G.; Andricopulo, A. D. Molecular docking and structure-based drug design strategies. *Molecules* **2015**, *20* (7), 13384−421.
(24) Wang, Z.; Sun, H.; Yao, X.; Li, D.; Xu, L.; Li, Y.; Tian, S.; Hou, T. Comprehensive evaluation of ten docking programs on a diverse set of protein-ligand complexes: the prediction accuracy of sampling power and scoring power. *Phys. Chem. Chem. Phys.* **2016**, *18* (18), 12964−75.
(25) Solis-Vasquez, L.; Tillack, A. F.; Santos-Martins, D.; Koch, A.; LeGrand, S.; Forli, S. Benchmarking the Performance of Irregular Computations in AutoDock-GPU Molecular Docking. *Parallel Comput* **2022**, *109*, 102861.
(26) Trott, O.; Olson, A. J. AutoDock Vina: improving the speed and accuracy of docking with a new scoring function, efficient optimization, and multithreading. *J. Comput. Chem.* **2010**, *31* (2), 455−61.
(27) Ding, J.; Tang, S.; Mei, Z.; Wang, L.; Huang, Q.; Hu, H.; Ling, M.; Wu, J. Vina-GPU 2.0: Further Accelerating AutoDock Vina and Its Derivatives with Graphics Processing Units. *J. Chem. Inf Model* **2023**, *63* (7), 1982−1998.
(28) Liu, N.; Xu, Z. Using LeDock as a Docking Tool for Computational Drug Design. *IOP Conf. Ser. Earth Environ. Sci.* **2019**, *218*, 012143.
(29) Zhang, X.; Gao, H.; Wang, H.; Chen, Z.; Zhang, Z.; Chen, X.; Li, Y.; Qi, Y.; Wang, R. PLANET: A Multi-objective Graph Neural Network Model for Protein-Ligand Binding Affinity Prediction. *J. Chem. Inf Model.* **2024**, *64*, 2205.
(30) Zhirui, L.; Ronghui, Y.; Xiaodi, H.; Y, X. DeepDock: Enhancing Ligand-protein Interaction Prediction by a Combination of Ligand and Structure Information. *2019 IEEE BIBM* **2019**, 311−317.
(31) Davies, M.; Nowotka, M.; Papadatos, G.; Dedman, N.; Gaulton, A.; Atkinson, F.; Bellis, L.; Overington, J. P. ChEMBL web services: streamlining access to drug discovery data and utilities. *Nucleic Acids Res.* **2015**, *43* (W1), W612−20.
(32) Gaulton, A.; Hersey, A.; Nowotka, M.; Bento, A. P.; Chambers, J.; Mendez, D.; Mutowo, P.; Atkinson, F.; Bellis, L. J.; Cibrian-Uhalte, E.; Davies, M.; Dedman, N.; Karlsson, A.; Magarinos, M. P.; Overington, J. P.; Papadatos, G.; Smit, I.; Leach, A. R. The ChEMBL database in 2017. *Nucleic Acids Res.* **2017**, *45* (D1), D945−D954.
(33) Zdrazil, B.; Felix, E.; Hunter, F.; Manners, E. J.; Blackshaw, J.; Corbett, S.; de Veij, M.; Ioannidis, H.; Lopez, D. M.; Mosquera, J. F.; Magarinos, M. P.; Bosc, N.; Arcila, R.; Kiziloren, T.; Gaulton, A.; Bento, A. P.; Adasme, M. F.; Monecke, P.; Landrum, G. A.; Leach, A. R. The ChEMBL Database in 2023: a drug discovery platform spanning multiple bioactivity data types and time periods. *Nucleic Acids Res.* **2024**, *52* (D1), D1180−D1192.
(34) Mysinger, M. M.; Carchia, M.; Irwin, J. J.; Shoichet, B. K. Directory of useful decoys, enhanced (DUD-E): better ligands and decoys for better benchmarking. *J. Med. Chem.* **2012**, *55* (14), 6582−94.
(35) Chen, L.; Cruz, A.; Ramsey, S.; Dickson, C. J.; Duca, J. S.; Hornak, V.; Koes, D. R.; Kurtzman, T. Hidden bias in the DUD-E dataset leads to misleading performance of deep learning in structure-based virtual screening. *PLoS One* **2019**, *14* (8), No. e0220113.
(36) Cleves, A. E.; Jain, A. N. Structure- and Ligand-Based Virtual Screening on DUD-E(+): Performance Dependence on Approximations to the Binding Pocket. *J. Chem. Inf Model* **2020**, *60* (9), 4296−4310.
(37) Kohnke, B.; Kutzner, C.; Grubmuller, H. A GPU-Accelerated Fast Multipole Method for GROMACS: Performance and Accuracy. *J. Chem. Theory Comput* **2020**, *16* (11), 6938−6949.
(38) Loschwitz, J.; Jackering, A.; Keutmann, M.; Olagunju, M.; Olubiyi, O. O.; Strodel, B. Dataset of AMBER force field parameters of drugs, natural products and steroids for simulations using GROMACS. *Data Brief* **2021**, *35*, 106948.
(39) Rastelli, G.; Del Rio, A.; Degliesposti, G.; Sgobba, M. Fast and accurate predictions of binding free energies using MM-PBSA and MM-GBSA. *J. Comput. Chem.* **2010**, *31* (4), 797−810.
(40) Genheden, S.; Ryde, U. The MM/PBSA and MM/GBSA methods to estimate ligand-binding affinities. *Expert Opin Drug Discov* **2015**, *10* (5), 449−61.

https://doi.org/10.1021/acsmedchemlett.4c00511
ACS Med. Chem. Lett. 2025, 16, 410−419

(41) Abbasi, M.; Mansourian, M.; Oskouie, A. A.; Taheri, S.; Mahnam, K. In-silico study MM/GBSA binding free energy and molecular dynamics simulation of some designed remdesivir derivatives as the inhibitory potential of SARS-CoV-2 main protease. *Res. Pharm. Sci.* **2024**, *19* (1), 29−41.
(42) Yang, H.; Lou, C.; Sun, L.; Li, J.; Cai, Y.; Wang, Z.; Li, W.; Liu, G.; Tang, Y. admetSAR 2.0: web-service for prediction and optimization of chemical ADMET properties. *Bioinformatics* **2019**, *35* (6), 1067−1069.

https://doi.org/10.1021/acsmedchemlett.4c00511
ACS Med. Chem. Lett. 2025, 16, 410−419